Quasi-Periodic Pulsations During the impulsive phase of a C1.8 Confined Flare

Yingjie Luo[1]

[1]Center for Solar-Terrestrial Research, New Jersey Institute of Technology (YL863@NJIT.EDU)

Introduction

Quasi-Periodic Pulsations (QPPs): periodic variations in flux

During solar flares, QPPs:
• Universal in nearly all phases of the flare.
• Cover nearly the whole bands from radio to gamma-ray emissions.
• Period differs from sub-seconds to several minutes.
• Massive mechanisms are widely discussed, with no general scenario for complicated cases.

Significance: A good indicator of the modulations of the flare energy release or transport processes.

During the impulsive of a C1.8 confined flare on February 18, 2016, X-ray and radio QPPs are detected. Utilizing the radio spectroscopic imaging technique provided by Karl G. Jansky Very Large Array (VLA), we found four distinct periodic radio sources in 1.0-2.0 GHz. We present detailed studies of these different sources and discuss their physical nature in this report.

Scientific Objectives

The main scientific objective is to find out the physical nature of the spatially and periodically different radio sources.

What's triggering:
• High-resolution spatially and temporally observations are available, which is rare and highly demanded in previous QPPs reports.
• The association between different radio emissions and X-Ray emissions is of great interest, may indicate essential energy transport processes.

Observations

Radio: QPPs are observed in nearly whole bands from VLA (Figure 1). Except for several strong pulsations, some weak pulsations and fine bursts are also detected, which are later confirmed from distinct radio sources. In a pity, no other solid concurrent radio observations to help us determine the bandwidth of the radio emission.

X-Ray: Fermi/GBM and RHESSI (partly) cover the impulsive phase. Pulsations are detected (Figure 1).

EUV: Failed eruptions are seen in SDO/AIA 171 (Figure 2), and apparent cooling down processes are observed during the decay phase.
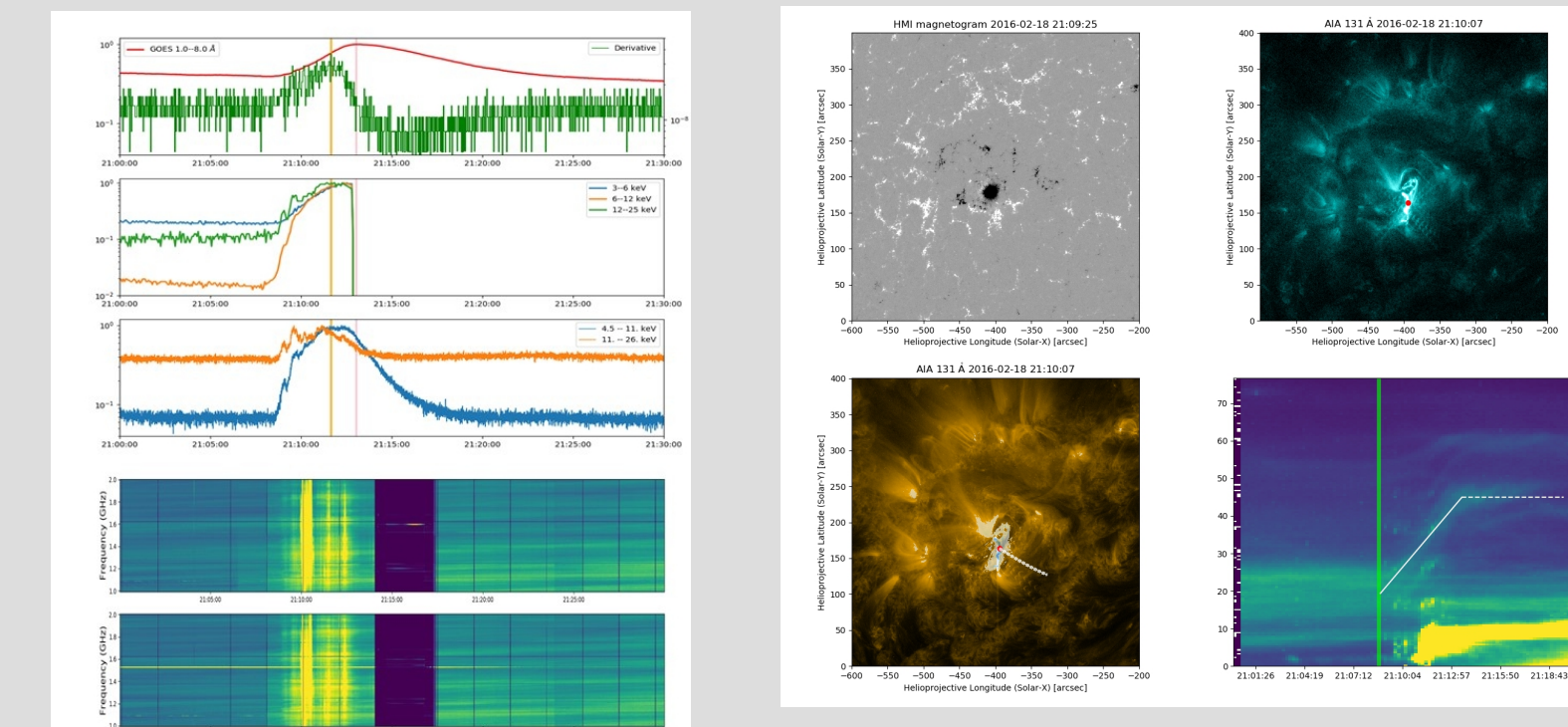

Figure 1. The upper three panels are GOES, RHESSI, and FERMI/GBM temporal profile. The lower two panels are VLA cross-power dynamic spectrum.

Figure 2. The top left is the SDO/HMI image, indicating a circular ribbon. SDO/AIA 131 image shows the flare arcades with an X-Ray looptop source. The lower two panels trace the failed eruption.

Distinct Radio sources

Utilizing the radio spectroscopic imaging technique, we can obtain a 4D image cube, thus generate a spatially-resolved 'vector' dynamic spectrum (Figure 3). VLA shows four distinct radio sources, and we list their characteristics in Table 1. We classified the radio sources as two groups for the following discussion.

	Intensity	Polarizations	Periods	Bands	Living Time
Strong QPPs (I)	Can reach 20 MK	RCP, typically DOP 40- 50%, up to 80%	~6s	Nearly full bands	~20 seconds later, lasts ~50 seconds
North Footpoint (II)	~ 4 MK	RCP	~29-43 s	1.2 – 1.8 GHz	Along with the loop top source
South Footpoint (III)	~ 2 MK	LCP	~27 -46 s	<1.5 GHz	Along with the loop top source
Loop top (IV)	~ 3 MK	Weakly Polarized	~25~37 s	1.1 -- 1.6 GHz	First detected, lasts over 3 minutes

Table 1. Characteristics of radio sources.
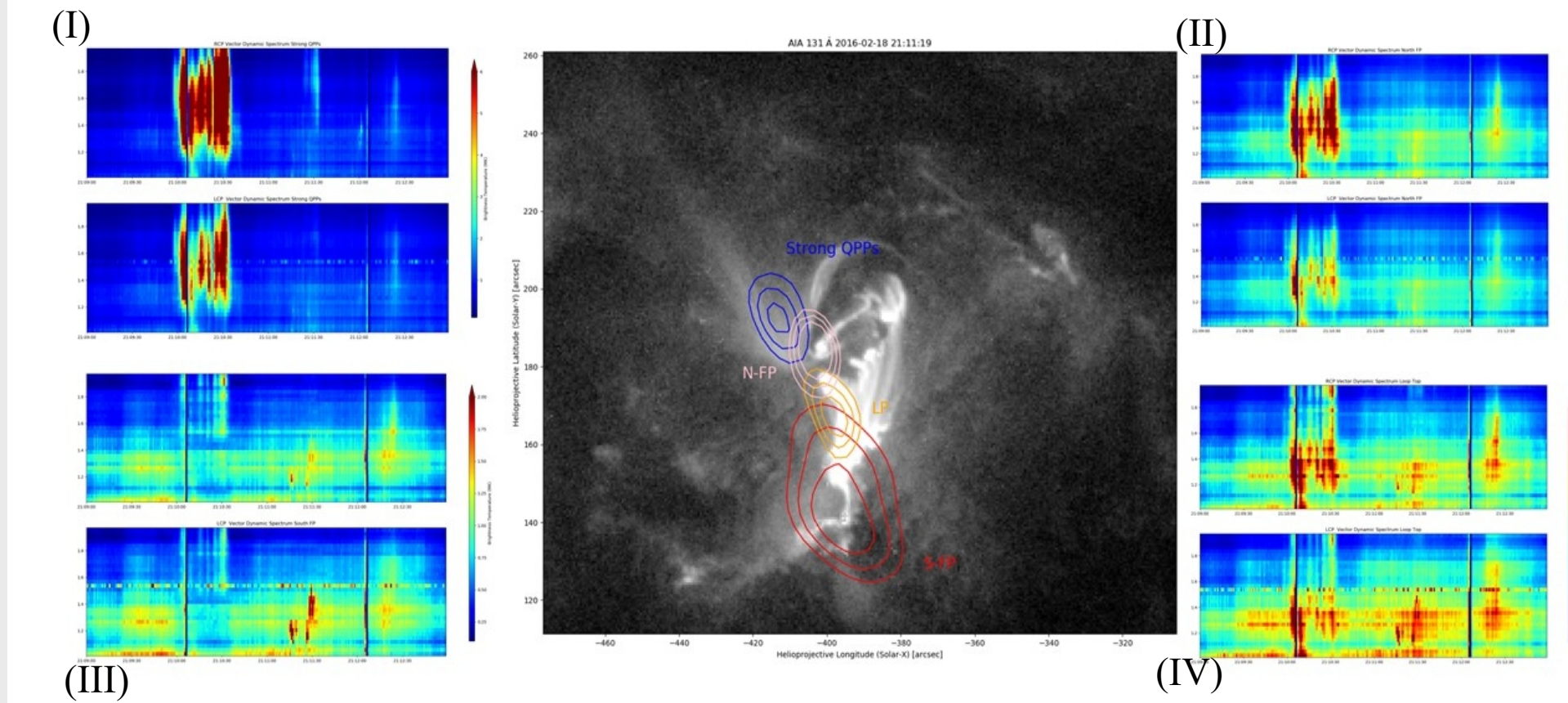

Figure 3. Vector Dynamic spectrum of 4 distinct radio sources.

Radio Source I: Strong QPPs

To discuss the possible mechanisms of strong QPPs, we present NLFFF extrapolation and try to locate the radio sources into the extrapolated magnetic structure. We show an exampled multi-frequency centroids in Figure 5. Owing to the projection effect, the radio sources can be anywhere along the line of sight in 3D volume (Figure 7 and 9). Here we discuss three candidate mechanisms. One is Incoherent Gyrosynchrotron emission, and the other two are coherent plasma emission and ECME.
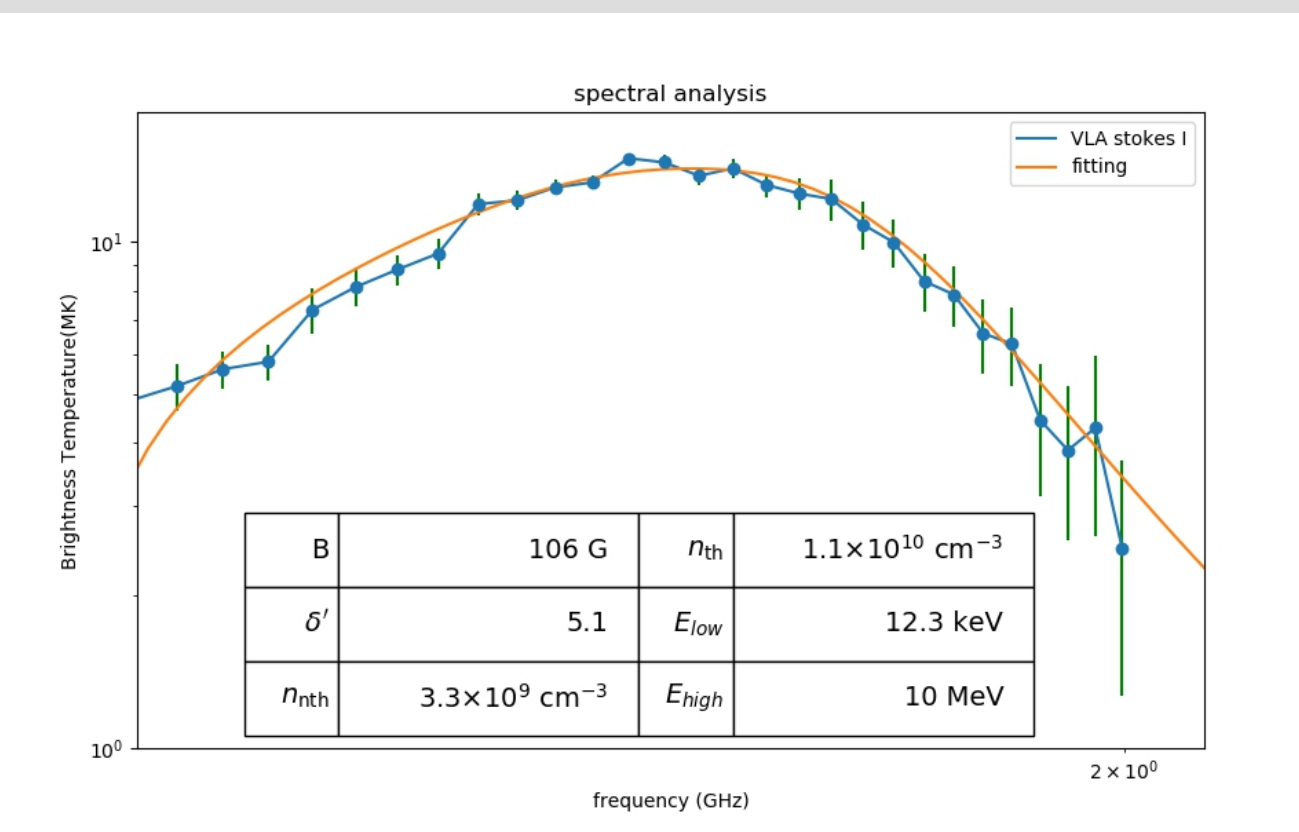

Figure 4. An exampled Gyrosynchrotron fitting of stokes I during the strong QPPs. The results show that B~106 G, $e_{th} \sim 1.1 \times 10^{10}\ cm^{-3}$, $e_{nth} \sim 3.3 \times 10^9\ cm^{-3}$, all are reasonable in corona.

B	106 G	n_{th}	$1.1 \times 10^{10}\ cm^{-3}$
δ'	5.1	E_{low}	12.3 keV
n_{nth}	$3.3 \times 10^9\ cm^{-3}$	E_{high}	10 MeV

Figure 5. Exampled centroids of the pulsations. Blue to red indicates increasing frequency. Size of each dot represent the flux intensity.
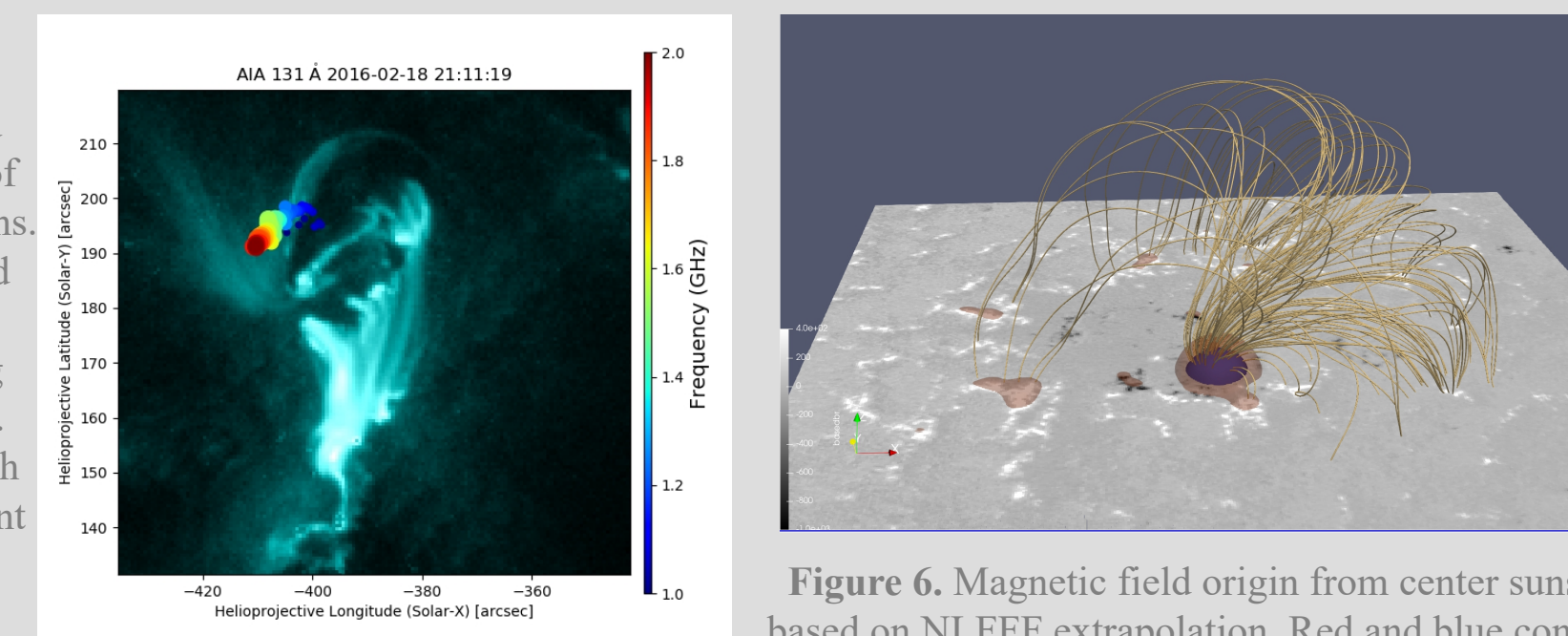

Figure 6. Magnetic field origin from center sunspot based on NLFFF extrapolation. Red and blue contours represent the magnetic field strength of 179 and 357 G.

Gyrosynchrotron: We got some good results in fitting Stokes I spectrum (an example in Figure 4). However, we met some difficulties in using a simple homogeneous model to fit the polarized spectrum.

Plasma emission: For plasma radiation, $f_p \approx 8980 \times \sqrt{n_e}$, Assuming fundamental emission, $n_e \sim 1.24 - 4.96 \times 10^{10}\ cm^{-3}$, Assuming 2nd harmonic emission, $n_e \sim 0.31 - 1.24 \times 10^{10}\ cm^{-3}$. We find a possible magnetic tube in Figure 7 and plot a possible scale height profile in Figure 8.
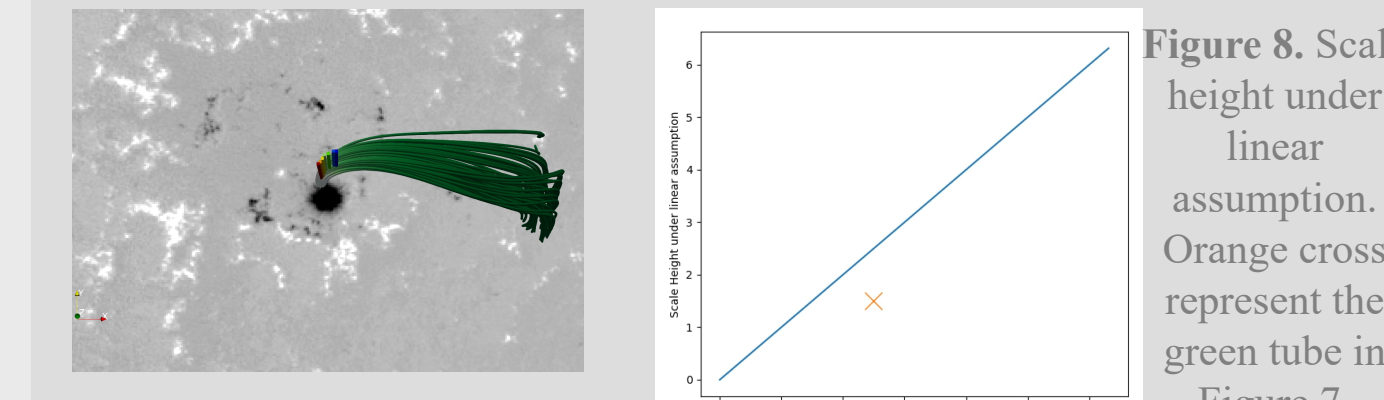

Figure 7. Magnetic tube following the radio centroids.

Figure 8. Scale height under linear assumption. Orange cross represent the green tube in Figure 7.

ECME: ECME triggers at $f \sim s f_B$, where electron gyrofrequency $f_B = 2.8 \times 10^6 B$. Considering the maser growth rate decrease very fast as harmonic number s increase, we only take s=1 and 2 into consideration. Recalling the frequency of pulsations 1-2 GHz, $B = f/(2.8 \times 10^6\ s)$. B ranges 357~714 (fundamental, s=1) and 179~357 (harmonic, s=2). A possible magnetic tube is shown in Figure 9.

We prefer two coherent emissions here, and further investigations are in the future plan.

Figure 9. Possible magnetic tube contours. The radio sources locate between two contours, indicating the emissions emit at second harmonic electron gyrofrequency.

Radio Source II, III, and IV: Weak QPPs

We put sources II, III, and IV together into the discussion as they locate along the flare arcades. We apply the cross-correlation check between radio emissions and X-ray emissions (Figure 10 and 11). The results show that the looptop radio emission is more correlated with the X-Ray emission, which is expected.

We speculate the looptop source comes from gyrosynchrotron emission, and the conjugate footpoints sources come from reconnected downflow.
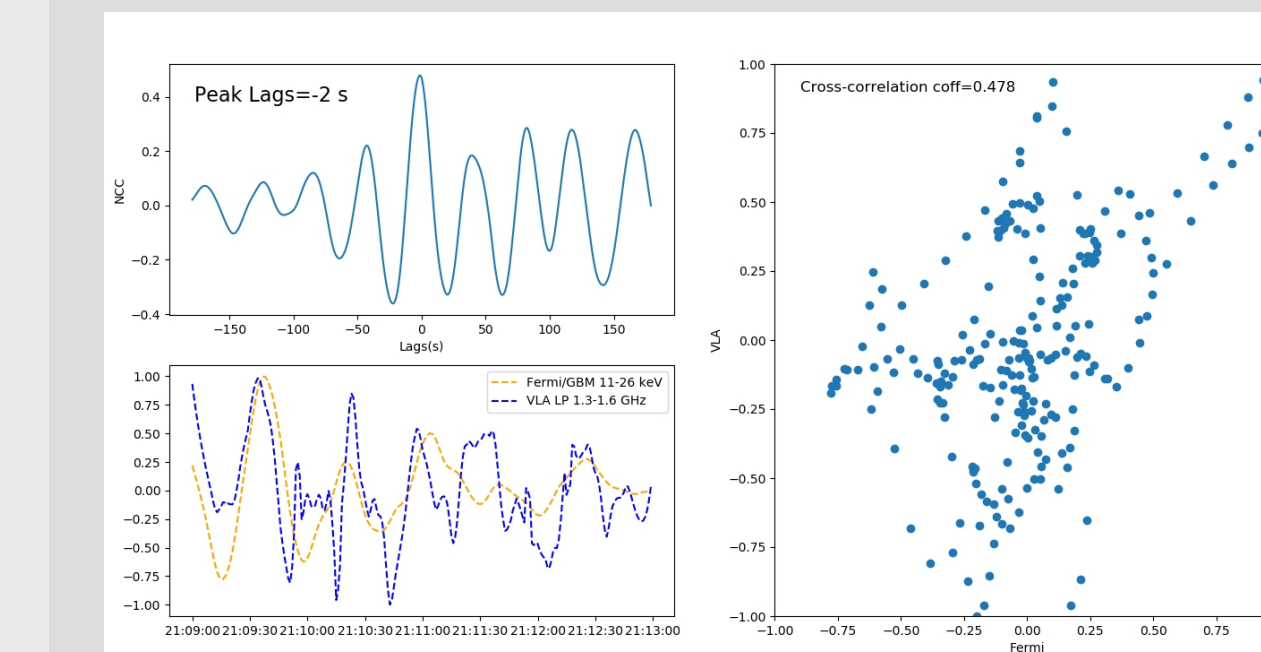

Figure 10. Cross-Correlation between loop top radio source and Fermi/GBM 11-26 keV. They are moderately correlated (NCC ~0.48).
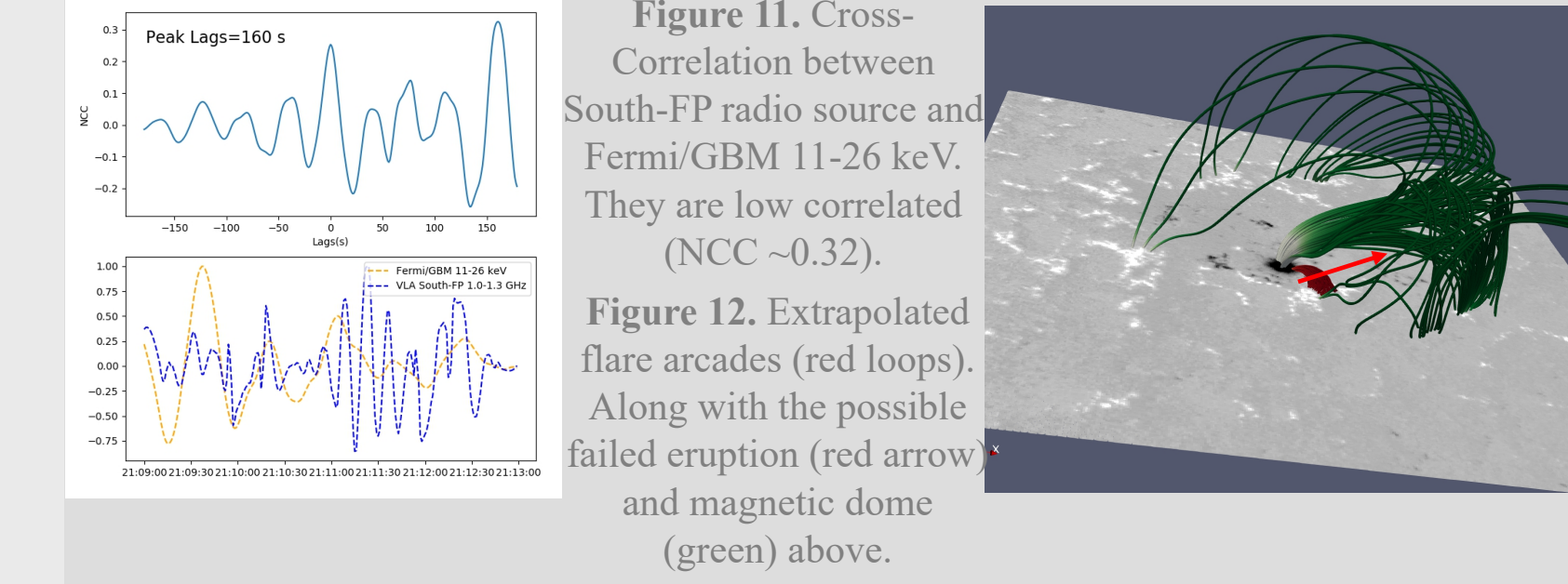

Figure 11. Cross-Correlation between South-FP radio source and Fermi/GBM 11-26 keV. They are low correlated (NCC ~0.32).

Figure 12. Extrapolated flare arcades (red loops). Along with the possible failed eruption (red arrow and magnetic dome (green) above.

DISCUSSION/ Future Plans

In previous sections, we show the characteristics of different radio emissions and try to locate them into the extrapolated magnetic field. We briefly discussed the mechanisms for each source. Another issue of great interest is how the energy release and transport to generate these different radio sources.

We show a schematic diagram in Figure 13. For radio sources II, III, and IV, it is likely consistent with the CSHKP flare model. Magnetic reconnection occurs, downflows trigger the looptop and two conjugate footpoint sources, which is consistent with concurrent X-ray emission. The upward outflow is unable to break the strapping magnetic dome, shown as failed eruption. Some of the accelerated electrons come into the west-east magnetic tube above. They later transport to another footpoint with a stronger magnetic field and trapped. The strong pulsations are then triggered. We prefer two different mechanisms that drive the periodic behaviors. Periodic reconnection may lead to the weak QPPs with a longer period, while MHD oscillations in the particle-injected magnetic tube are responsible for the strong QPPs.
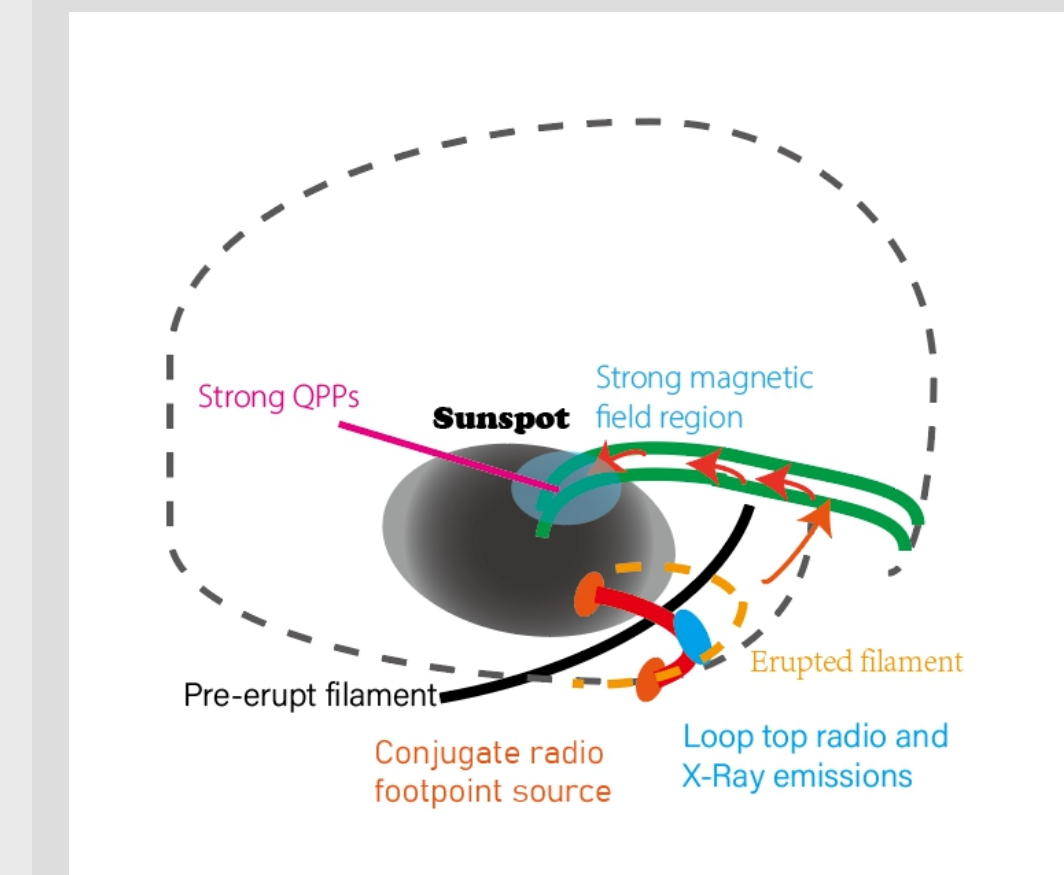

Figure 13. Schematic diagram. Magnetic reconnection brightens the flare arcades and triggers associated X-ray and radio emissions. The erupted filament hit upper magnetic loops and inject some energetic particles into them. These particles are trapped in one of the footpoint to trigger strong QPPs.

Preliminary results identify the preferred mechanism for each radio emission and manifest a highly possibly existing causal relationship between them through energy transport. The future work contains a detailed investigation of mechanisms of emission and drivers of oscillation. Also, we need to check the evolution of the emissions once again, in which we may find essential hints ignored before.